Interannual variability of snowmelt in the Sierra Nevada and Rocky Mountains, United States: Examples from two alpine watersheds

Steven M. Jepsen,[1] Noah P. Molotch,[2,3] Mark W. Williams,[2] Karl E. Rittger,[4] and James O. Sickman[5]

Received 7 June 2011; revised 1 December 2011; accepted 31 December 2011; published 23 February 2012.

[1] The distribution of snow and the energy flux components of snowmelt are intrinsic characteristics of the alpine water cycle controlling the location of source waters and the effect of climate on streamflow. Interannual variability of these characteristics is relevant to the effect of climate change on alpine hydrology. Our objective is to characterize the interannual variability in the spatial distribution of snow and energy fluxes of snowmelt in watersheds of a maritime setting, Tokopah Basin (TOK) in California's southern Sierra Nevada, and a continental setting, Green Lake 4 Valley (GLV4) in Colorado's Front Range, using a 12 year database (1996–2007) of hydrometeorological observations and satellite-derived snow cover. Snowpacks observed in GLV4 exhibit substantially greater spatial variability than in TOK (0.75 versus 0.28 spatial coefficient of variation). In addition, modeling results indicate that the net turbulent energy flux contribution to snowmelt in GLV4 is, on average, 3 times greater in magnitude (mean 29% versus 10%) and interannual variability (standard deviation 17% versus 6%) than in TOK. These energy flux values exhibit strong seasonality, increasing as the melt season progresses to times later in the year ($R^2 = 0.54$–0.77). This seasonality of energy flux appears to be associated with snowmelt rates that generally increase with onset date of melt (0.02 cm d^{-2}). This seasonality in snowmelt rate, coupled to differences in hydrogeology, may account for the observed differences in correspondence between the timing of snowmelt and timing of streamflow in these watersheds.

Citation: Jepsen, S. M., N. P. Molotch, M. W. Williams, K. E. Rittger, and J. O. Sickman (2012), Interannual variability of snowmelt in the Sierra Nevada and Rocky Mountains, United States: Examples from two alpine watersheds, *Water Resour. Res.*, *48*, W02529, doi:10.1029/2011WR011006.

1. Introduction

[2] Snowmelt is an important and dynamically changing water resource in mountainous regions around the world [*Arnell*, 1999; *Barnett et al.*, 2005]. In the western United States, much of the precipitation (39%–67%) falls as snow [*Serreze et al.*, 1999] in a proportion depending on both latitude and elevation [*Bales et al.*, 2006]. Springtime melt of this snow largely controls the timing and magnitude of runoff, the prediction of which is essential for the proper timing of dam releases for municipal and agricultural water supplies, hydropower, and flood control [*Molotch et al.*, 2004]. Accurate water supply assessments in snowpacks is challenging because of the high spatial variability of snow water equivalent (SWE) in alpine environments [*Erickson et al.*, 2005; *Winstral et al.*, 2002; *Elder et al.*, 1991, 1995].

[3] Future changes in climate are expected to have a geographically varying effect on snowmelt because of the close coupling between energy and water fluxes [*Cayan*, 1996; *Bales et al.*, 2006]. Seasonal shifts in snowmelt timing will influence the timing of streamflow [*Gleick*, 1987] and the sustainability of water resources [*Knowles and Cayan*, 2004], making knowledge of the interannual variability in snowmelt energy fluxes in different regions important for understanding climate change effects on hydrology. Similarly, potential future changes in the spatial distribution of SWE could impact the geochemistry of surface waters [*Williams and Melack*, 1991a; *Melack and Sickman*, 1995], nutrient cycling processes [*Brooks and Williams*, 1999; *Williams et al.*, 2009], and aquatic ecosystems [*Bunting et al.*, 2010; *Molotch et al.*, 2008].

[4] Previous works have improved the understanding of physical processes affecting the partitioning of energy fluxes during snowmelt [e.g., *Male and Granger*, 1981; *Morris*, 1989; *Pohl et al.*, 2006]. Simulations of these processes have been facilitated through the development of numerical snowmelt models [e.g., *Anderson*, 1976; *Jordan*, 1991; *Lehning et al.*, 2006]. In parallel, several works have

[1]U.S. Geological Survey, Denver, Colorado, USA.
[2]Department of Geography and Institute of Arctic and Alpine Research, University of Colorado at Boulder, Colorado, USA.
[3]Jet Propulsion Laboratory, California Institute of Technology, Pasadena, California, USA.
[4]Donald Bren School of Environmental Science and Management, University of California, Santa Barbara, California, USA.
[5]Department of Environmental Sciences, University of California, Riverside, California, USA.

0043-1397/12/2011WR011006

improved the ability to estimate fractional snow cover extent from satellite [*Dozier*, 1989; *Rosenthal and Dozier*, 1996; *Painter et al.*, 2009]. These improvements have facilitated development of the snow reconstruction method, in which SWE is calculated retroactively by integrating modeled snowmelt over the period of satellite-observed snow cover. This method was used by *Martinec and Rango* [1981] to reconstitute snow in remote, inaccessible regions using Landsat images and a temperature index snowmelt model. Subsequent studies have refined the method [*Brubaker et al.*, 1996; *Cline et al.*, 1998] and have applied it to analyze the spatial distribution of SWE and snowmelt during 1–2 year periods [*Cline et al.*, 1998; *Molotch and Margulis*, 2008; *Molotch*, 2009]. These improvements, however, have not gained adequate use for the analysis of interannual variability of SWE and snowmelt.

[5] The objective of this study is to characterize the interannual variability of SWE and energy flux components of snowmelt in alpine watersheds of a maritime and continental setting. Twelve years (1996–2007) of detailed hydrometric observations are utilized from two of the most intensively studied alpine watersheds in North America; the Tokopah Basin in the southern Sierra Nevada, California (maritime influence), and Green Lake 4 Valley in the Colorado Front Range (continental influence). The following questions are addressed: (1) How variable is snow accumulation in these two climatologically different watersheds? (2) How variable is the partitioning of snowmelt energy between the radiative and turbulent fluxes? (3) How does the timing of snowmelt compare to the timing of streamflow in these watersheds? The findings of this study have implications for the influence of climate variability in alpine maritime and continental settings on the interannual variability of SWE, snowmelt and streamflow.

2. Study Area

[6] The Tokopah Basin (TOK) is an alpine watershed of maritime influence located in Sequoia National Park, California (Figure 1 and Table 1) and representative of high-elevation watersheds in the Sierra Nevada [*Tonnessen*, 1991]. Annual precipitation is highly variable, ranging from less than 1 m to greater than 2 m [*Williams and Melack*, 1991b], occurring mainly as snow (75%–90%) (*Stephenson* [1988] as discussed by *Tonnessen* [1991]). Soils are thinly distributed and generally restricted to small areas of the valley floor [*Molotch and Bales*, 2006], and forest cover is generally absent (Table 1). Data from three meteorological stations (EML, TPL, and M3) and a streamflow gaging station, located at the TOK outlet (Marble Fork, MF), were used for this study (Figure 1). Annual snow surveys have sampled SWE at maximum accumulation off and on since 1985 (Table 2).

[7] The Green Lake 4 Valley (GLV4) is an alpine watershed of continental influence located in the Colorado Front Range (Figure 1 and Table 1) and is typical of the high-elevation environments in this area [*Williams et al.*, 1996]. Niwot Ridge is a prominent interfluve that forms the northern boundary of the surrounding Green Lakes Valley (GLV) and is home to the Niwot Ridge Long Term Ecological

Table 1. Geographical Information for Tokopah Basin (TOK) and Green Lake 4 Valley (GLV4)

Parameter	TOK	GLV4
Location	36°36.9′N, 118°39.2′W	40°3.1′N, 105°37.8′W
Area	19.1 km^2	2.2 km^2
Elevation range	2620–3490 m	3560–4024 m
Mean elevation	3150 m	3750 m
Mean slope	17°	28°
Exposed bedrock[a]	51%	30%
Exposed talus[a]	6%	34%
Forest cover[b]	5%	0.3%
Typical date of maximum snowpack[a,c]	early April	early to middle May
Percent area above (below) z_stn_range[d]	45% (5%)	52% (0%)

[a] *Erickson et al.* [2005].
[b] National Land Cover Database 2001, http://www.mrlc.gov.
[c] *Molotch and Bales* [2006].
[d] Here z_stn_range indicates the elevation range of meteorological stations.

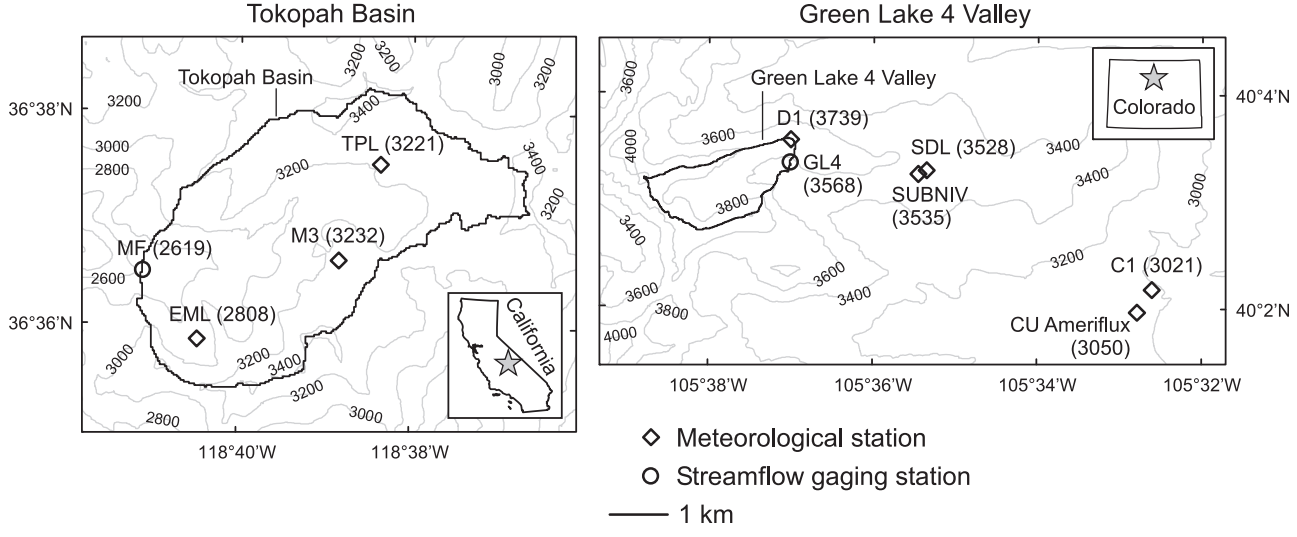

Figure 1. Location map of Tokopah Basin, California, and Green Lake 4 Valley, Colorado. Station elevations (m) are shown in parentheses.

Table 2. Statistics of Snow Surveys Conducted in TOK and GLV4 Between 1996 and 2007[a]

	TOK						GLV4					
Year	Date	d_{ave}	N_d	ρ_{ave}	N_ρ	CV	Date	d_{ave}	N_d	ρ_{ave}	N_ρ	CV
1996	11 Apr	273	319	454	3	0.39	4 May	-	-	382	6	-
1997	9 Apr	256	429	465	10	0.37	14 May	256[b]	193[b]	398	5	0.73[b]
1998	6 May	361	352	467	42 (40)	0.32	20 May	242[b]	370[b]	494	5	0.69[b]
1999	17 Apr	169	204	406	15 (12)	0.38	12 May	221[b]	532[b]	359	4	0.88[b]
2000	15 Apr	256	11	480	2 (1)	0.19	3 May	213[b]	655[b]	461	4	0.88[b]
2001	28 Apr	191	54	440	1	0.29	9 May	188[b]	511[b]	419	4	0.74[b]
2002	30 Apr	176	95	-	-	0.42	1 May	123[b]	447[b]	386	2	1.09[b]
2003	-	-	-	-	-	-	14 May	222[b]	527[b]	376	5	0.75[b]
2004	15 Apr	174	86	-	-	0.5	12 May	132	517	445	5	1
2005	2 Apr	405	21	403	1	0.38	10 May	215	427	380	3	0.75
2006	-	-	-	-	-	-	11 May	152	483	405	1	0.98
2007	3 Apr	133	83	-	-	0.37	10 May	124	695	418	5	1.06

[a]Symbols are as follows: d_{ave}, mean depth (cm); N_d, number of depth measurements; ρ_{ave}, mean snow density (kg m^{-3}); N_ρ, number of density measurements (number of Federal sampler cores in parentheses); CV, spatial coefficient of variation. A dash indicates no data.
[b]Data from *Erickson et al.* [2005].

Research Station. Climate data have been collected continuously along Niwot Ridge since the early 1950s [*Williams et al.*, 1996] (Niwot Ridge LTER, http://culter.colorado.edu/NWT/index.html). GLV receives about 1 m of precipitation annually, mainly as snow (~80%) [*Williams et al.*, 1996]. Soils are limited to the riparian zone of the valley floor and vegetation is limited to grasses and shrubs [*Meixner et al.*, 2000]. Data from five meteorological stations (D1, Saddle (SDL), C1, Subnivean (SUBNIV), and CU Ameriflux) and a streamflow gaging station, located at the GLV4 outlet (GL4), were used for this study (Figure 1). Maximum SWE was measured during annual snow surveys, each averaging 446 depth measurements and producing a total of 5300 measurements (Table 2).

3. Methods

[8] A reconstruction model was used to compute snowmelt over remotely sensed, snow covered areas [*Molotch*, 2009]. Modeled snow-atmosphere energy exchange, required for predicting snowmelt, was determined from energy balance calculations, spatially interpolated meteorological parameters and modeled shortwave radiation. Grids of SWE at maximum accumulation were formed by integrating modeled snowmelt between the dates of maximum snow accumulation and satellite-observed snow disappearance. These grids were compared to grids of observed SWE, formed using regression methods and comprehensive snow surveys conducted each spring. Supplementary data on snowmelt were obtained from the Niwot SNOTEL Site 663 (Natural Resources Conservation Service), located 8.5 km east of GLV4, and the Giant Forest station, CA (U.S. Army Corp of Engineers), located 11.5 km southwest of TOK. Modeled snowmelt timing was characterized to reveal interannual variability in water inputs to both watersheds. Differences in timing between modeled snowmelt and observed streamflow were evaluated to explore possible differences between the two watersheds in terms of residence time. The proportion of the net radiative and net turbulent fluxes to total modeled energy of snowmelt was compared for TOK and GLV4. These comparisons pertain to snow-covered areas during all hours of the melt season, defined to begin and end at 10% and 90% cumulative melt, respectively. Each component of the methods is further described below.

3.1. SWE Reconstruction Model

[9] Maximum snow water equivalent, SWE_0, for each grid cell was reconstructed by summing snowmelt increments modeled between the date of maximum SWE (i.e., snow survey dates; Table 2) and date of snow disappearance [*Molotch*, 2009]:

$$SWE_0 = \sum_{j=1}^{n} M_j, \tag{1}$$

where M_j is an increment in snowmelt (m) during time step j (hourly) and n is the total number of time steps between the dates of maximum SWE and snow disappearance. Spatially averaged values of modeled SWE_0 were compared to observed values using the Nash-Sutcliffe coefficient of model efficiency [*Nash and Sutcliffe*, 1970], expressed as "percent variability in mean SWE explained by the model." New snowfall was not included in equation (1) because it was insignificant relative to that occurring prior to the date of maximum SWE accumulation.

[10] Incremental snowmelt values, M_j (equation (1)), were determined from

$$M_j = M_{p,j} SCA_j, \tag{2}$$

where $M_{p,j}$ is an increment in potential snowmelt (i.e., snowmelt assuming complete snow cover) and SCA_j is the fraction of the grid cell covered by snow during time step j, determined by interpolating satellite-observed FSCA with respect to cumulative potential snowmelt [*Molotch*, 2009]. An increment in potential snowmelt was determined from

$$M_{p,j} = E_{p,j} (\rho_w L_{sl})^{-1} t_{sph} \tag{3}$$

$$E_{p,j} = \max \left[0, \min \left[\left(\sum_{k=0}^{j} Q_{net,k} \right), Q_{net,j} \right] \right], \tag{4}$$

where ρ_w is the density of liquid water, L_{sl} is the latent heat of fusion (3.34×10^5 J kg^{-1}), t_{sph} is the number of seconds per hour (3600 s h^{-1}), $Q_{net,j}$ is the net energy flux (W m^{-2}) to the snow surface during time step j, and $E_{p,j}$ is the energy available for snowmelt after accounting for cold content, defined as the difference (absolute value thereof) between the internal energy of subfreezing snow and snow at 0°C. Cold content of snow was accounted for as follows. At midnight of each day, cold content was initialized to zero. A running total was kept of the net energy flux to the snow surface from hour $k = 0$ (at midnight) to $k = j$ (summation in equation (4)). Values of this sum when negative were set equal to the magnitude of cold content. During any given time step, the energy available for snowmelt was equated to the value of $Q_{net,j}$ in excess of the cold content (equation (4)). When cold content was not accounted for during preliminary model testing, melt spikes were frequently computed during winter daylight hours. This result was not considered physically accurate since the snow was likely below the melting point during those times.

[11] The net energy flux during time step j, $Q_{net,j}$, is given by

$$Q_{net,} = (1 - \alpha_{\mathrm{SNOW}})K_j + L_j^* + Q_{H,j} + Q_{L,j}, \qquad (5)$$

where α_{SNOW} is the albedo of snow, K_j is downwelling shortwave radiation, L_j^* is net longwave radiation, $Q_{H,j}$ is the sensible heat flux, and $Q_{L,j}$ is the latent heat flux. Ground heat flux was excluded from equation (5) because it is generally insignificant during the snowmelt season [*Marks et al.*, 1992]. The snow surface temperature used for calculating upwelling longwave and the turbulent fluxes was prescribed as a 1 h lag function of air temperature, constrained to 0°C or below [*Cline and Carroll*, 1999]. The positive (negative) direction of all fluxes is defined as being directed toward (away from) the snow surface. Forcings and parameterizations to derive the aforementioned energy flux terms are adopted from methods of previous studies, including spatial interpolation of meteorological parameters [*Cline et al.*, 1998; *Molotch et al.*, 2008; *Molotch*, 2009], modeling of shortwave radiation [*Dozier*, 1980; *Dickinson et al.*, 1993; *Cline and Carroll*, 1999; *Molotch*, 2009], longwave radiation [*Idso*, 1981; *Hodges et al.*, 1983; *Cline and Carroll*, 1999], and turbulent fluxes [*Jordan*, 1991; *Morris*, 1989; *Marks and Dozier*, 1992]. Details of these methods are provided in Appendix A.

3.2. Fractional Snow-Covered Area

[12] Fractional snow-covered area (FSCA) grids at 30 m resolution were constructed from Landsat 5 and 7 images using the Thematic Mapper Snow Covered Area and Grain Size algorithm (TMSCAG) [*Painter et al.*, 2009]. The first satellite image used each year was the one displaying the greatest overall snow cover; all available images with reasonably low cloud cover were used for the remainder of the year (through August). The number of satellite images used per year for TOK ranged from 7 to 9 and averaged 7.5, and for GLV4 ranged from 3 to 9 and averaged 6.1. FSCA was normalized by the viewable gap fraction to correct for forest canopy [*Molotch and Margulis*, 2008], with forest cover fraction obtained from the National Land Cover Database 2001 (http://www.mrlc.gov). At each model time step, FSCA values were interpolated with respect to cumulative modeled melt between the nearest cloud-free satellite images [*Molotch*, 2009]. Cloud masks were used to flag FSCA grid cells that were considered to be cloud covered. When this occurred, preceding and subsequent FSCA grids were searched until a cloud-free grid cell for interpolation was located. Grid cells were considered to be cloud covered when all of the following conditions were satisfied: $R_{52} > 0.4$, $R_1 > 0.25$, $R_5 > 0.25$, where R_i is the Landsat-derived reflectance in band i and R_{52} the ratio of R_5 to R_2. This simplification of the regression tree approach of *Rosenthal and Dozier* [1996] produced cloud images that corresponded well with observations from Landsat R-G-B (bands 5-4-2) images.

3.3. Hydrometric Measurements

[13] Existing snow survey data sets and statistical methods were used to obtain grids of observed maximum SWE (see *Molotch et al.* [2005] for TOK and *Erickson et al.* [2005] for GLV4). Snow survey dates were aimed to coincide with the typical date of maximum SWE, and measurement locations were generally chosen to sample a range of elevation, slope and aspect. Year to year differences in data availability necessitated the use of different statistical methods. During 1996–1999, the TOK snow surveys were extensive, each collecting over 200 depth measurements (Table 2). For these years, snow depth grids at maximum SWE accumulation were constructed through spatial interpolation of snow survey measurements using binary regression tree models [*Molotch et al.*, 2005]. TOK surveys after 1999 were not sufficiently comprehensive to apply binary regression trees (Table 2). Taking advantage of recurring snow depth patterns in the TOK [*Leydecker et al.*, 2001], snow depth grids after 1999 were obtained by fitting the measured depths to the 1996–1999 average grid (Appendix B). Snow density was measured during the TOK surveys using a combination of snow pits and Federal sampler cores (Table 2).

[14] The GLV4 snow depth grids for all years were provided by the deterministic grids of *Erickson et al.* [2005]. These were based on about 500 measurements per year from 1997–2003; grids for the other years were based on the multiyear regression of *Erickson et al.* [2005]. 1997–2003 values of mean snow depth in GLV4 at maximum accumulation were obtained from *Erickson et al.* [2005], and for the remaining years were obtained from the Niwot Ridge snow surveys (http://culter.colorado.edu/NWT/). Snow density was measured during the GLV4 surveys in snow pits on south and north facing aspects (Table 2).

[15] All snow depth grids were multiplied by the FSCA image nearest in time to the snow survey to account for snow-free areas. Final SWE grids were created by multiplying snow depth grids by the observed mean specific gravity (ratio of observed snow density to that of water). For years when no snow densities were measured, the multiyear average of specific gravity was used.

[16] SWE recorded at the Niwot SNOTEL and Giant Forest station were used as independent indicators of the timing of snowfall and snowmelt in GLV4 and TOK, respectively. Hourly values of stream discharge at the TOK outlet were obtained from the Marble Fork (MF) streamflow gaging station (Figure 1). Daily values of stream discharge from GLV4 were obtained from the Green Lake 4 (GL4)

streamflow gaging station (Niwot Ridge LTER: http://culter.colorado.edu/NWT/). The integration period for the stream and snowmelt centroids was 1 March to 31 August.

4. Results

4.1. Energy Fluxes and Timing of Snowmelt

[17] The magnitudes and interannual variability of modeled turbulent energy fluxes are a factor of three greater in GLV4 than TOK (Figures 2a and 2b). The net turbulent flux (sensible plus latent heat) to snow in TOK averaged spatially over all melt seasons is +3.9 W m^{-2}, providing on average 10% of the energy for snowmelt (Figure 2a). This proportion ranges from 0% in 2002 (when latent and sensible heat fluxes were equal in magnitude but opposite in sign) to 18% in 2006, with an interannual variability (standard deviation) of 6% (Figure 2a). The mean net turbulent flux to snow in GLV4 over all years modeled is +15.6 W m^{-2}, providing on average 29% of the energy for snowmelt (Figure 2b). This proportion ranges from 3% in 2007 to 51% in 1999, with an interannual variability of 17% (Figure 2b). Both watersheds show the same multiyear mean value in modeled net longwave radiation (−68 W m^{-2}) and similar means in modeled net shortwave radiation: 114 W m^{-2} for TOK and 108 W m^{-2} for GLV4 (Figures 2c and 2d).

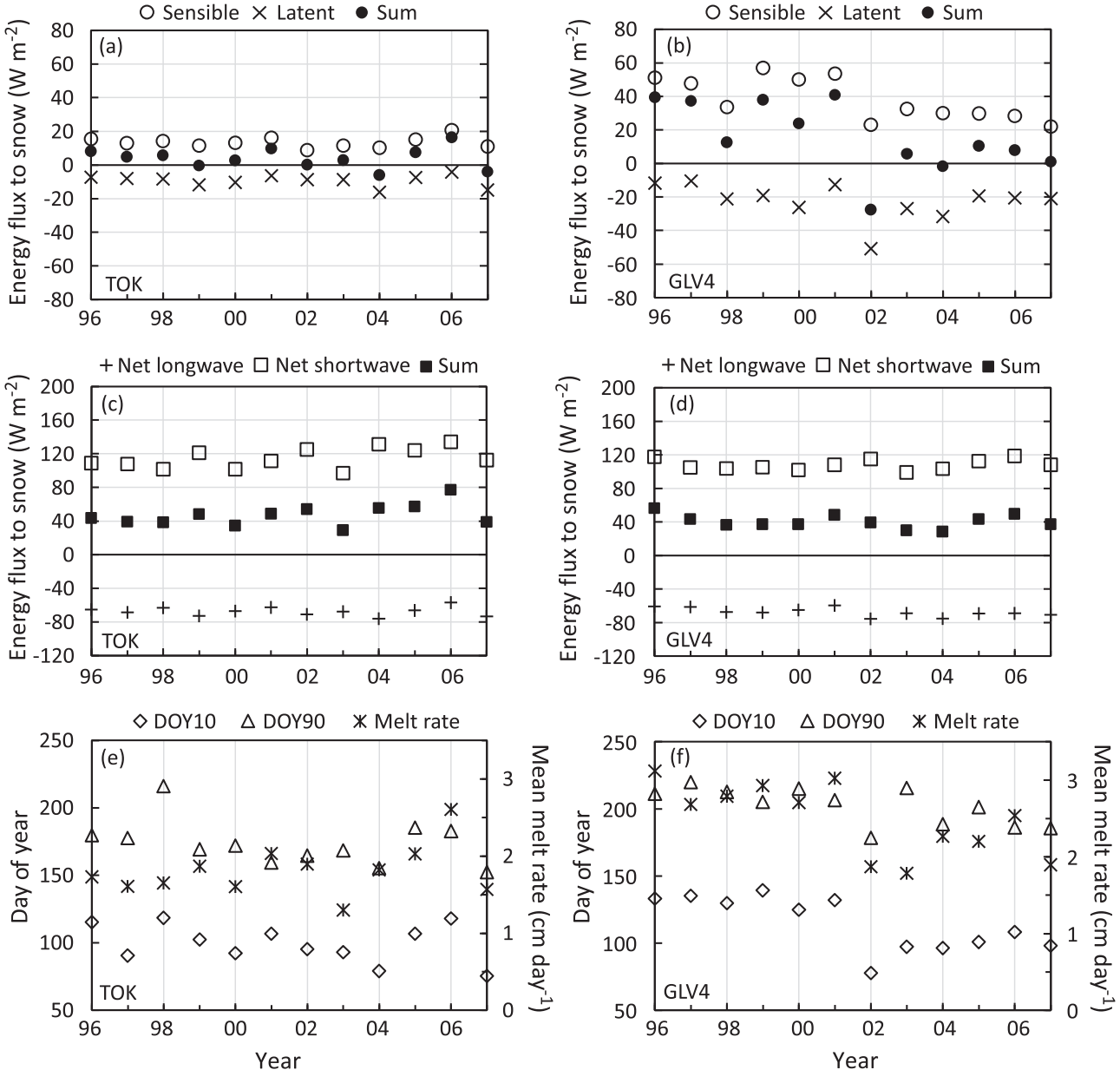

Figure 2. (a–d) Modeled energy fluxes to snow averaged spatially and temporally during each melt season (10%–90% cumulative melt) for Tokopah Basin (left) and Green Lake 4 Valley (right). (e, f) Modeled timing of each melt season (DOY10 is the start, and DOY90 is the end) and melt rates averaged spatially and temporally.

[18] The model results and observations both indicate decreasing snowmelt rates for melt seasons beginning earlier in the year (Figures 2e, 2f, 3a and 3b). Modeled start dates of snowmelt are also well correlated to modeled turbulent energy flux (R^2 = 0.54–0.77, Figures 3c and 3d). The curves of turbulent flux versus snowmelt timing are 2–3 times steeper for GLV4 than TOK (Figures 3c and 3d), illustrating the greater interannual variability of turbulent fluxes at the continental site.

4.2. SWE Variability and Model SWE Errors

[19] Observed maximum SWE, spatially averaged over the watersheds, varies by a factor of 3.2 in TOK (49–158 cm) and 4.4 in GLV4 (27–119 cm) (Table 3). The quantity of SWE in TOK generally follows gradients in elevation and aspect, with greater values on the higher-elevation north facing aspects and lower values on the lower-elevation south facing aspects (Figure 4, left). Bands of high SWE accumulation in the southeastern watershed, which were reproduced by the model, are known to occur as a result of avalanche redistribution [*Elder et al.*, 1991]. The greatest SWE accumulations in GLV4 generally occur along a corridor extending from the southwestern to north central area of the watershed (Figure 4, right). Lower accumulations tend to occur over the windswept slopes in the northwest and southeast (Figure 4, right). SWE distributions are markedly more heterogeneous in GLV4 than TOK (Figure 4). Spatial coefficients of variation in GLV4 range from 0.38 to 1.45 (mean of 0.75, standard deviation (SD) of 0.29), while values in TOK range from 0.24 to 0.34 (mean of 0.28, SD of 0.04) (Table 3).

Table 3. Statistics of Grids of Observed Maximum SWE[a]

	TOK		GLV4	
Year	μ	CV	μ	CV
1996	115.9	0.29	86.5	0.71
1997	114.6	0.26	97.6	0.45
1998	158.2	0.25	118.5	0.51
1999	64.5	0.28	70.0	0.64
2000	89.9	0.25	62.8	0.87
2001	79.7	0.25	65.8	0.66
2002	66.8	0.32	27.3	1.45
2003	-	-	77.2	0.38
2004	63.9	0.34	56.6	0.77
2005	148.9	0.24	62.6	0.67
2006	-	-	43.9	1.00
2007	48.5	0.33	44.9	0.93

[a]SWE, snow water equivalent; μ, mean (cm); CV, spatial coefficient of variation. A dash indicates no data.

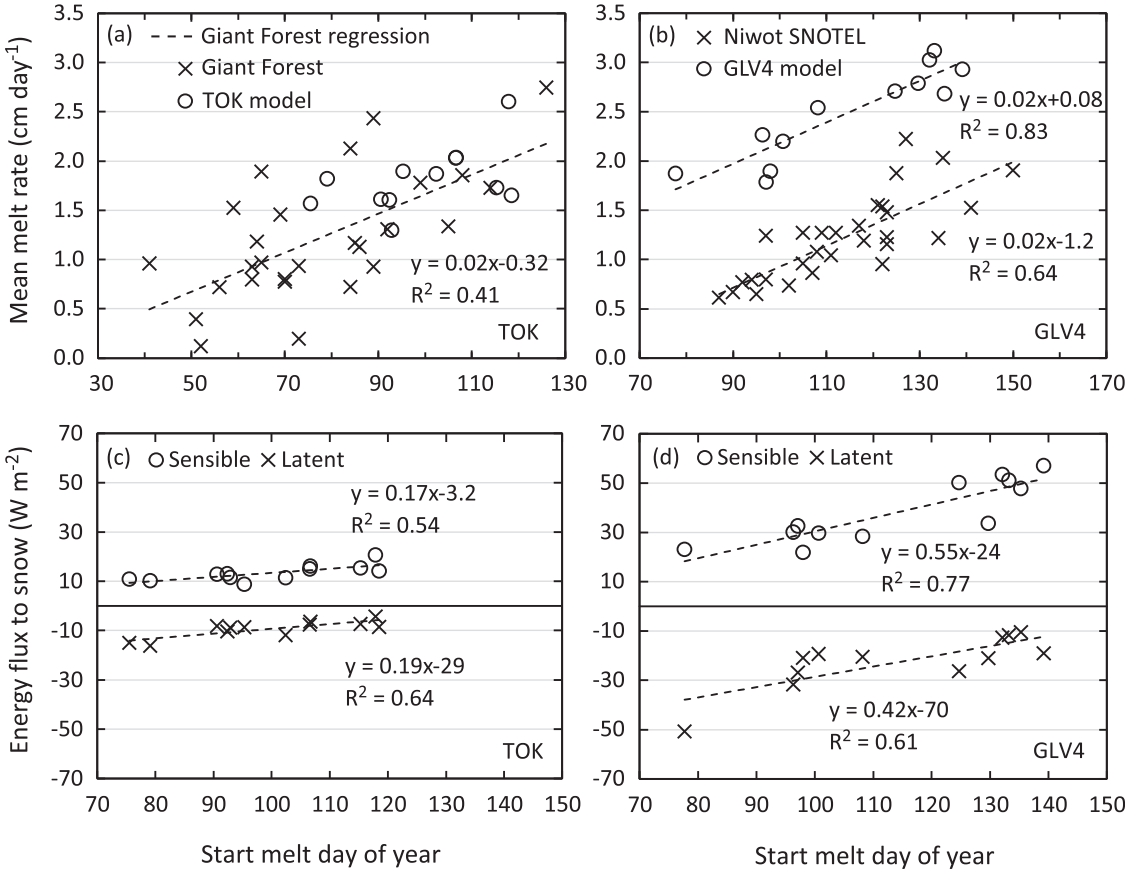

Figure 3. Modeled and observed relationships between timing of snowmelt, melt rate, and turbulent energy flux to snow. (a, b) Modeled melt rates averaged spatially and temporally during the melt season versus start date of melt, with observed rates (Giant Forest, 1975–2009; Niwot, 1982–2010). (c, d) Modeled sensible and latent heat fluxes averaged spatially and temporally during the melt season versus start date of melt.

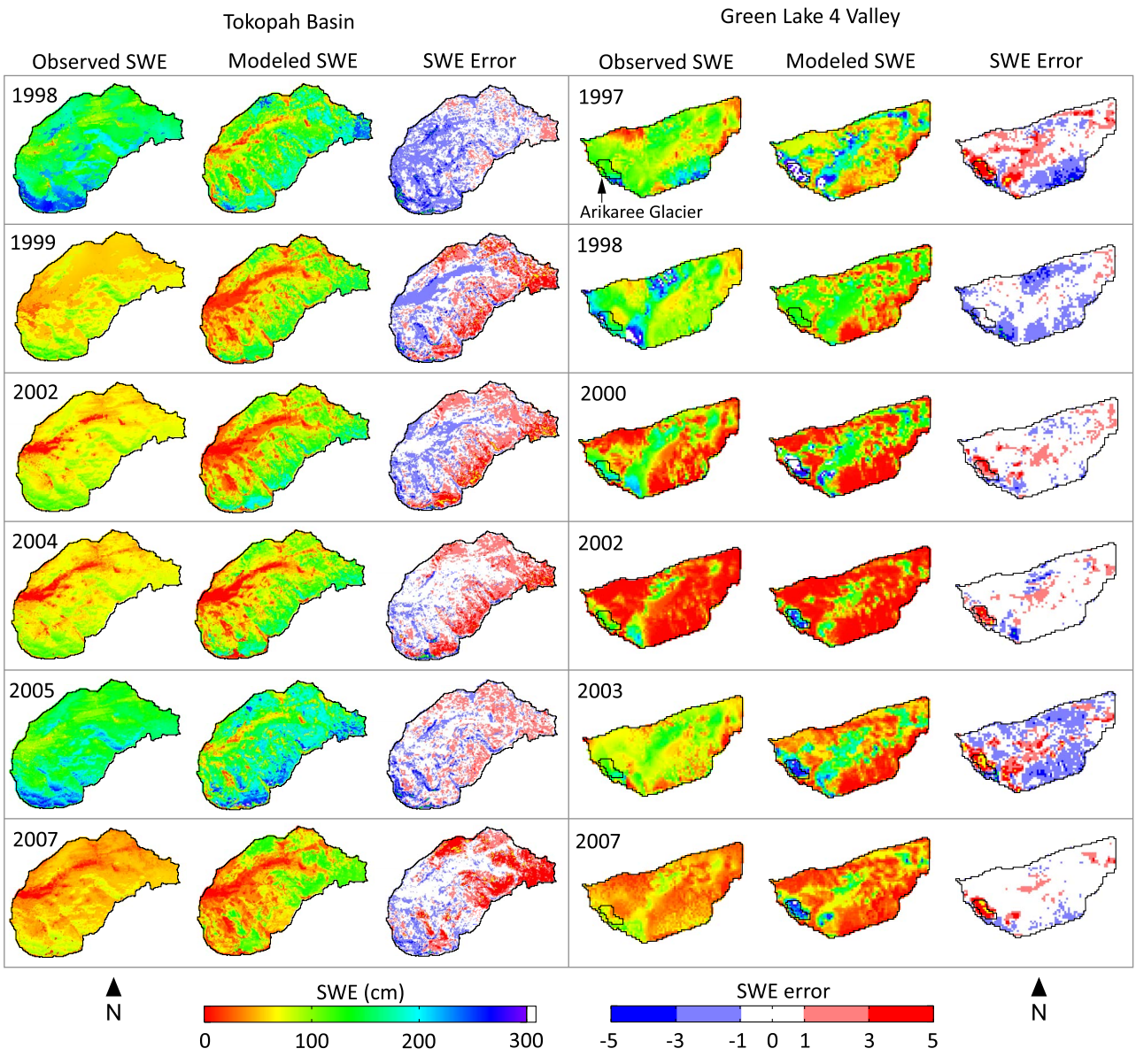

Figure 4. Grids of observed and modeled maximum snow water equivalent (SWE) and model SWE error. The SWE error grids are normalized by the spatial standard deviation of SWE, given by $(SWE_{mod} - SWE_{obs})/\sigma$, where SWE_{mod} is the modeled SWE grid (shown), SWE_{obs} is the observed SWE grid (shown), and σ is the year-specific, spatial standard deviation of SWE_{obs}, found from Table 3 and the relation $\sigma = \mu CV$.

[20] Model SWE errors are generally within 3 standard deviations (spatial) of the observed SWE and tend to form spatial patterns that persist from year to year (Figure 4). Model overestimates in TOK SWE persist in the eastern and southeastern watershed (Figure 4, left). These overestimates are most prevalent during the years of lowest SWE (i.e., 1999, 2002, 2004, and 2007). Model underestimates in TOK SWE occur at the lower elevations and on north facing cliff bands in the southern watershed (arcuate-shaped features in Figure 4, left). Model overestimates in GLV4 SWE occur predominantly along a narrow northeast trending corridor where the greatest SWE accumulations occur (Figure 4, right). Underestimates in SWE tend to occur in the southern and northern portions of the GLV4 watershed, where wind scour often reduces snow accumulation. These underestimates are most pronounced in years with relatively deep snow in these areas (i.e., 1997, 1998, and 2003; Figure 4, right).

[21] The TOK model explains 79% of the observed interannual variability in mean SWE (Figure 5, left). Model SWE errors for the different years range from −23% of observed SWE in 1998 to +27% of observed SWE in 2007 (Figure 5, left). The standard deviation of these errors for all years modeled is 18.3% about a mean of −0.1%. Model results for TOK tend to be high biased for years of relatively low SWE (Figure 5, left). The GLV4 model explains 60% of the observed interannual variability in mean SWE (Figure 5, right). Model SWE errors for the different years

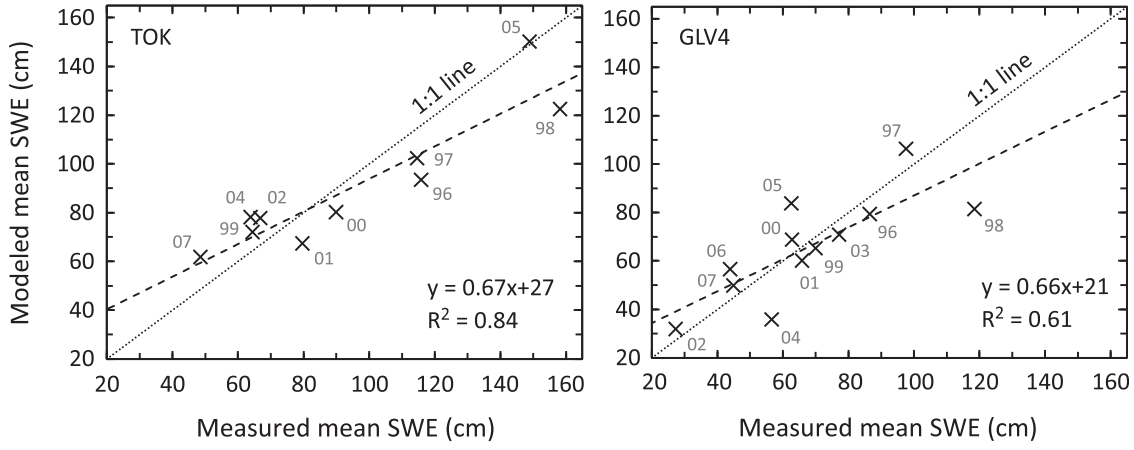

Figure 5. Modeled versus observed mean maximum SWE in TOK and GLV4, with years labeled.

range from −37% of observed SWE in 2004 to +34% of observed SWE in 2005 (Figure 5, right). The standard deviation of these errors for all years modeled is 21.6% about a mean of +0.8%.

4.3. Snowmelt and Streamflow Timing

[22] Modeled daily snowmelt in TOK correlates strongly to observed stream discharge, with R^2 values each year ranging from 0.70 to 0.85 and averaging 0.78 (p values <0.01) (Figure 6, top). Modeled snowmelt time series are displaced downward relative to the stream hydrographs for the drought years of 2004 and 2007, possibly in association with antecedent soil moisture deficits during dry periods. Daily modeled snowmelt and observed discharge in GLV4 are relatively decoupled compared to TOK, with R^2 values ranging from 0.00 to 0.28 and averaging 0.14 (p values ranging from <0.1 to 0.6) (Figure 6, bottom).

[23] For both watersheds, correlations between the centroid dates of modeled snowmelt and observed stream discharge are stronger than correlations between daily flux values. The TOK snowmelt and stream discharge centroids show a similar range, 65 and 56 days, respectively, and strong correlation (R^2 = 0.97, p value <0.01; Figure 7, left). The GLV4 snowmelt centroids also correlate strongly to the stream discharge centroids (R^2 = 0.70, p value <0.01), but exhibit substantially different ranges (i.e., 42 versus 9 days) (Figure 7, right). These findings suggest that the timing of snowmelt and streamflow is relatively decoupled in GLV4 relative to TOK.

[24] For some years in GLV4, substantial snow-covered area depletion occurs prior to the rising limb of streamflow (e.g., 1996, 2002, and 2006) (Figure 6, bottom). This is especially apparent for 2002, where about 50% of the maximum snow-covered area disappears prior to increased discharge at the streamflow gauge. In contrast, the rising limb of the TOK hydrographs generally coincides temporally with snow cover depletion (Figure 6, top). These direct observations are consistent with the reconstruction model in suggesting that snowmelt and streamflow are relatively decoupled in GLV4 (more in section 5).

4.4. Model Forcing Errors

[25] Shortwave model errors at EML, TPL, and C1 become more positive over the course of the study period (Figures 8b and 8e). Though reasons for this are unclear, sensor drift is one possibility. RMS model errors in TOK and GLV4 shortwave over the different years average 79 and 75 W m^{-2}, respectively (data not shown). RMS model errors in TOK and GLV4 longwave over the different years average 28 and 36 W m^{-2}, respectively (data not shown).

[26] Yearly averages (March–August) in the reduced residuals of meteorological observations are listed in Table 4. To demonstrate, the 1996 air temperature residual of +1.3°C at C1 indicates that the observation there is 1.3°C higher than the value predicted by interpolating with respect to elevation using the other stations. Values at M3 are equal and opposite in sign to those at TPL (as stations are nearly at the same elevation). Residuals at D1 are opposite in sign to values at SDL (Table 4), but 25%–50% greater in magnitude. The variance in observations across stations (Table 5) is substantially greater in magnitude than the sum of squares in residuals (Table 4), indicating a generally strong correlation of the meteorological parameters to elevation.

5. Discussion

[27] A main finding of this study is the observed relationship between timing of snowmelt, rate of snowmelt, and the contribution of the turbulent energy fluxes. Earlier melting snowpacks are observed to ablate more slowly (∼0.02 cm d^{-2}) and derive proportionally less energy from the turbulent energy fluxes. The proportion of these energy fluxes to the total energy flux during the melt season was on average three times greater (29% versus 10%) at the continental site (GLV4) than the maritime site (TOK), likely in association with wind speeds ∼3 times greater in the former (Table 5). Further studies considering different time periods, and utilizing different modeling approaches, are needed to determine whether or not these relationships are characteristic of continental and maritime snowpacks.

[28] *Cline* [1995] studied energy exchanges on Niwot Ridge during 1994, finding that the net turbulent flux provided 25% of the energy available for snowmelt. While this value is close to our reported 1996–2007 average of 29%, it is substantially lower than the value observed for 1999 (51%). This is explained as follows. First, snowmelt at the Niwot SNOTEL during year 1999 began about 18 days

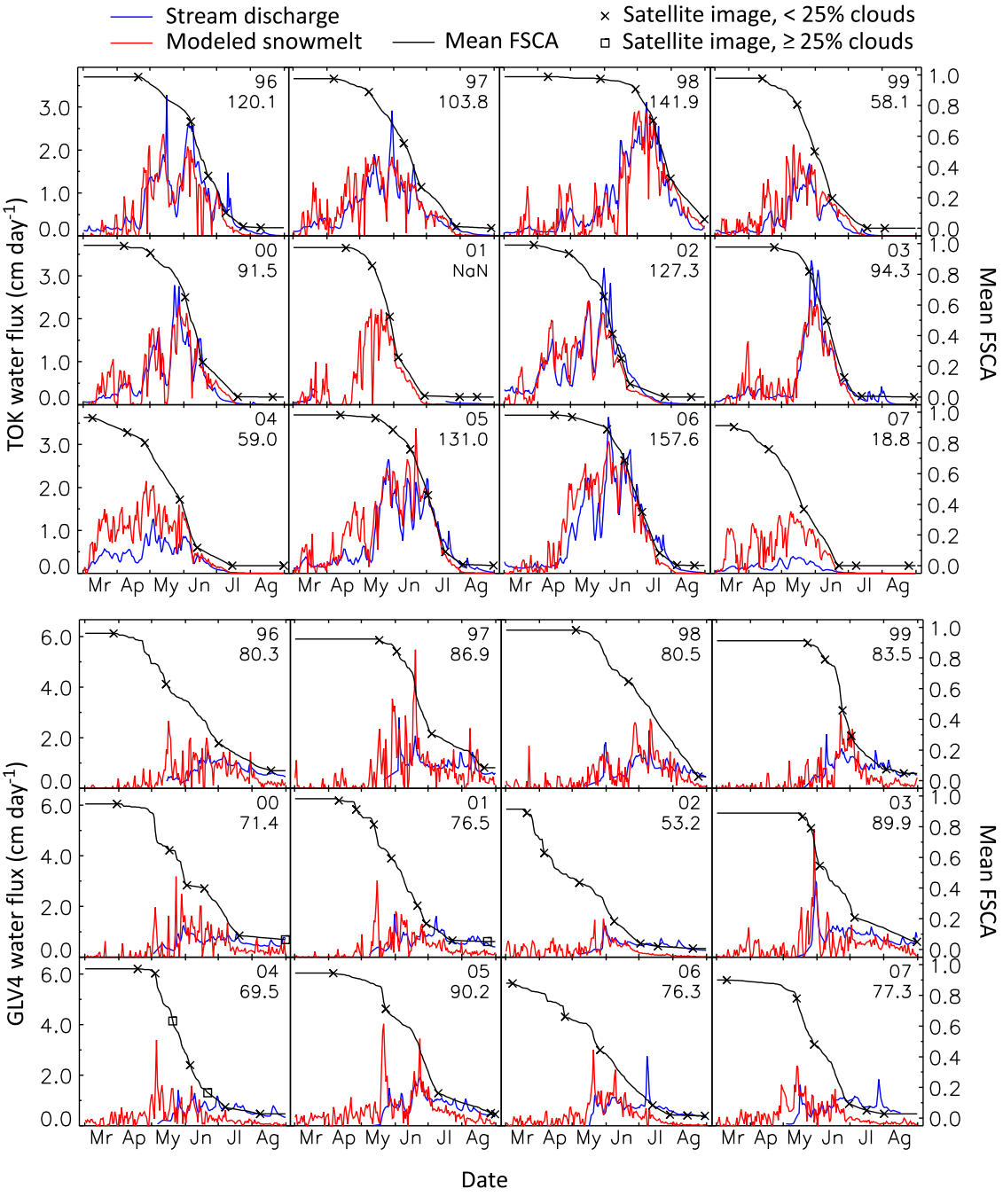

Figure 6. Modeled snowmelt and observed stream discharge normalized by watershed area (cm d^{-1}) for (top) TOK and (bottom) GLV4. Black lines show the mean watershed fractional snow-covered area (FSCA). In the right corner of each plot, the top number is year, and the bottom number is cumulative 1 March to 31 August stream discharge (cm). NaN indicates data not available.

after it did during 1994. On the basis of the correlation shown in Figure 3d, the contribution of net turbulent flux to snowmelt would have been substantially greater in 1999 than 1994. Second, the values reported in this study are spatially averaged over areas of variable solar radiation exposure, whereas the site on Niwot Ridge is topographically flat with relatively high exposure.

[29] Observations indicate substantially greater spatial variability of SWE in GLV4 than TOK (2.6:1 ratio in mean CV; Table 3). Higher wind speeds in GLV4 (~3 times; Table 5) are likely an important cause for this difference [*Luce et al.*, 1998; *Winstral et al.*, 2002; *Anderton et al.*, 2004; *Erickson et al.*, 2005]. The occurrence of late season, large snowfall events appears to be another factor influencing the high degree of SWE spatial variability in GLV4. The 2 years of lowest SWE spatial variability in GLV4, 1997 and 2003, experienced relatively large spring snowfall events on the basis of observations at the nearby Niwot SNOTEL (i.e., >8 cm water equivalent during any three consecutive days). In contrast, years with the highest

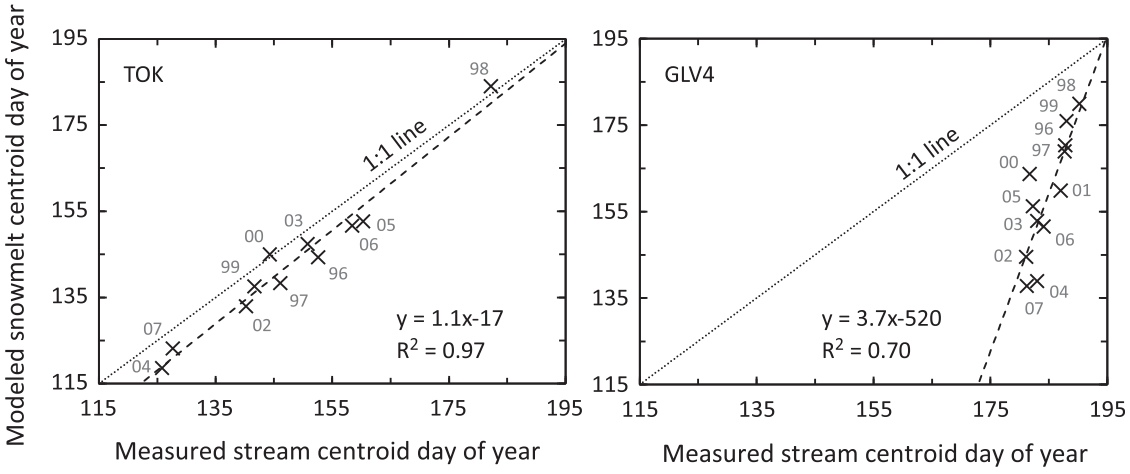

Figure 7. Interannual variability in timing of modeled snowmelt and observed stream discharge. The centroid day of year is the day of 50% cumulative 1 March to 31 August water flux (0 = 1 January). The points are labeled with years.

SWE spatial variability (i.e., 2000 and 2002) did not experience large spring snowfall events (i.e., <3 cm water equivalent). In general, snowfall during spring will be relatively high in density as a result of higher air temperatures as compared to midwinter [*Pomeroy et al.*, 1998; *Judson and Doesken*, 2000], possibly resulting in greater resistance to wind redistribution and thus lower spatial variability. Further work is needed to examine the wind conditions during these springtime snowfall events.

[30] Model SWE errors in this study are similar to previous applications of the SWE reconstruction technique. *Molotch* [2009] reported a mean SWE error of 23% for the Rio Grande headwaters of Colorado in years 2001 and 2002. This error is similar to our mean SWE errors for GLV4, ranging from −37% to +34% of the observed (about a mean and SD of about 1% and 22%, respectively). *Cline et al.* [1998] reported 6% mean SWE error from their model of the Emerald Lake watershed of TOK during year

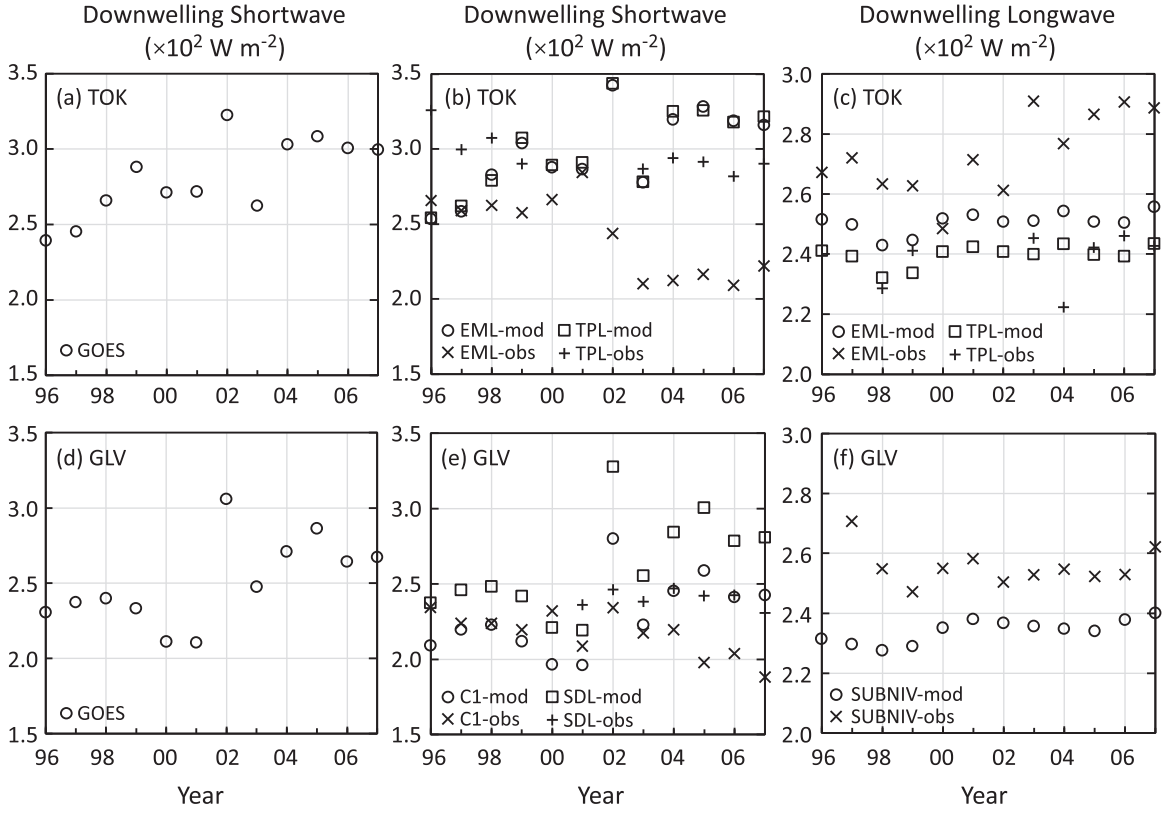

Figure 8. Values of observed (obs) and modeled (mod) downwelling shortwave and longwave radiation, averaged between 1 March and 31 August of each year.

Table 4. Reduced Residuals in Meteorological Forcings Used for the Reconstruction Model (1 March to 31 August Averages)[a]

	TPL (TOK)			C1 (GLV)			SDL (GLV)		
Year	T_a	V_w	P_w	T_a	V_w	P_w	T_a	V_w	P_w
1996	0.0	0.7	−0.1	1.3	−2.2	-	−0.4	0.6	-
1997	0.4	0.6	−0.1	1.2	−2.3	-	−0.4	0.7	-
1998	0.0	0.4	−0.1	1.0	−4.8	-	−0.3	1.4	-
1999	−0.3	0.6	−0.3	-	-	-	-	-	-
2000	-	-	-	-	-	-	-	-	-
2001	-	-	-	0.0	−1.7	−0.6	0.0	0.5	0.2
2002	-	-	-	−1.5	−1.5	−1.3	0.4	0.4	0.4
2003	−0.2	0.7	-	0.4	−0.8	−0.7	−0.1	0.2	0.2
2004	−0.2	0.5	-	−0.9	−2.9	0.7	0.3	0.9	−0.2
2005	−0.1	0.5	-	−0.9	−1.7	0.6	0.3	0.5	−0.2
2006	−0.2	0.5	-	−0.7	−1.8	0.7	0.2	0.5	−0.2
2007	−0.4	0.6	−0.6	−1.1	−2.0	1.0	0.3	0.6	−0.3

[a] T_a, air temperature (°C); V_w, wind speed (m s^{-1}); P_w, water vapor pressure in air (mbars). A dash indicates no data.

1993. In comparison, our mean SWE errors for TOK range from −23% to +27% of the observed SWE (about a mean and SD of ∼0% and 18%).

[31] Important sources of model error likely include (1) the method for determining cold content, (2) availability of cloud-free satellite images, and (3) model forcing accuracy. The method for determining cold content does not include the coupling between internal energy and mass of a snowpack. Thus, setting cold content to zero each night may have resulted in an overestimate of early season snowmelt, and an overestimate of melt during years with relatively large SWE (i.e., high cold content). Another source of model error is the availability of satellite images, with a possible overestimate in timing of snow disappearance by up to 2 weeks depending on cloudiness and satellite overpass schedule [*Molotch et al.*, 2010]. In regard to model forcing errors, the presence of only one meteorological station in GLV4 (D1 at the watershed boundary) is another possible source of error. More meteorological stations are needed in GLV4 to adequately predict local lapse rates and thereby effectively distribute model forcings.

Table 5. Average Monthly Air Temperature (T_a), Relative Humidity (RH), and Wind Speed (V_w) Observed at Each Meteorological Station During the Period of 1996–2007

	TOK								
	T_a (°C)			RH			V_w (m s^{-1})		
Month	EML	M3	TPL	EML	M3	TPL	EML	M3	TPL
Mar	0.1	−2.5	−2.5	51	53	48	1.8	2.8	3.4
Apr	0.9	−1.9	−2.0	57	60	59	1.7	2.8	3.3
May	6.5	3.7	3.2	54	56	56	1.4	2.3	2.8
Jun	10.7	8.2	7.9	50	52	52	1.4	2.1	2.7
Jul	15.0	12.3	12.4	47	48	44	1.5	2.1	2.7
Aug	14.1	11.9	11.7	43	44	41	1.4	2.2	2.8
	GLV								
	T_a (°C)			RH			V_w (m s^{-1})		
Month	C1	D1	SDL	C1	D1	SDL	C1	D1	SDL
Mar	−3.0	−9.0	−7.3	54	61	64	3.1	11.2	9.9
Apr	0.6	−5.1	−3.9	54	57	64	2.8	9.2	8.4
May	5.2	0.8	1.6	56	55	60	2.0	7.9	7.1
Jun	10.0	6.1	6.9	50	42	52	1.8	6.8	5.9
Jul	13.9	9.8	11.0	53	48	54	1.7	5.4	4.6
Aug	12.0	8.0	9.7	60	53	59	1.6	6.2	5.1

[32] Given that snowfall constitutes over 75% of the annual precipitation in both watersheds [*Williams et al.*, 1996; *Sickman et al.*, 2001], the timing of snowmelt is expected to play a major role in the timing of streamflow [*Clow*, 2010]. This is consistent with the high correlations found between the centroids of modeled snowmelt and observed stream discharge (Figure 7). However, the differences between the snowmelt and stream discharge centroids are substantially greater in GLV4 than TOK (Figure 7). This could reflect errors in the GLV4 model, or it could indicate in GLV4 a stronger influence from factors other than snowmelt timing on the timing of streamflow [*Williams et al.*, 2011]. One possible factor may be greater surface-groundwater interaction in GLV4 than TOK, the latter of which exhibits limited groundwater storage, shallow soils and relatively little talus compared to GLV4 (Table 1) [*Kattelmann and Elder*, 1991; *Huth et al.*, 2004; *Liu et al.*, 2004; *Molotch et al.*, 2008]. This may result in greater infiltration of snow meltwater in GLV4 than TOK, and hence a greater lag time between the centroids of snowmelt and stream discharge. Greater disparity between snowmelt and streamflow timing in GLV4 than TOK is also consistent with the observed differences in correspondence between snow cover depletion and stream discharge (Figure 6).

[33] The date of spring snowmelt in western North America has advanced earlier in the year by about 4 days $decade^{-1}$ since the 1950s, with higher air temperatures believed to be a cause [*Cayan et al.*, 2001; *Stewart et al.*, 2005; *Clow*, 2010]. Our results suggest that this may lead to slower melting snowpacks and a reduced contribution of turbulent energy flux to melt. Lower snowmelt rates would likely affect the partitioning of snowmelt between surface runoff and groundwater flow, and thus the lag time between snowmelt and streamflow. In watersheds with sufficient infiltration capacity and subsurface storage to accommodate snowmelt (e.g., GLV4), lower melt rates may result in deeper flow paths of snow meltwater and hence greater lag times. In watersheds with less infiltration capacity and subsurface storage, such as bedrock dominated TOK, lag times would likely be less sensitive to snowmelt rate because of higher runoff and shallower flow paths. These relationships would also affect evaporative losses of meltwater flowing to streams. Watershed hydrogeology would therefore mediate the effects of snowmelt timing and ablation rate on changes in streamflow as shown in previous studies [*Jefferson et al.*, 2008; *Tague and Grant*, 2009].

6. Conclusions

[34] Snow water equivalent (SWE) at the continental alpine site, Green Lake 4 Valley (GLV4), exhibits on average 3 times greater spatial variability (CV of 0.75 versus 0.28) and 7 times greater interannual variability in CV (standard deviation: 0.29 versus 0.04) than at the maritime site, Tokopah Basin (TOK). The modeled net turbulent flux contribution to snowmelt in GLV4 is on average three times greater in magnitude (mean of 29% versus 10%) and

interannual variability (standard deviation of 17% versus 6%) than in TOK. At both sites, the turbulent energy fluxes transition from more latent heat transfer from snow during years of earlier melt, to more sensible heat transfer to snow during years of later melt. This energy transition appears to be associated with snowmelt rates that increase by about 0.02 cm d^{-2} with respect to start date of melt. The observed timing of streamflow in GLV4 was relatively decoupled from the timing of modeled snowmelt in comparison to TOK. This may be a result of greater subsurface storage and infiltration capacity in GLV4, possibly acting in concert with seasonality in snowmelt rate. This leads to the interpretation that streamflow timing in watersheds supporting deeper flow paths of snowmelt may be somewhat buffered to changes in the timing of snowmelt.

Appendix A: Meteorological Forcings and Energy Fluxes

A1. Standard Meteorological Forcings

[35] Digital elevation models at 30 m resolution were used to spatially distribute model forcings. Hourly values of air temperature, relative humidity and wind speed for TOK were obtained from stations EML, TPL and M3 (Figure 1). Precipitation in TOK (for computing snow albedo) was taken to be spatially uniform at the value recorded at the Giant Forest station, located 11.5 km southwest of TOK at an elevation of 2027 m. Hourly values of air temperature, relative humidity, wind speed and precipitation for GLV4 were obtained from stations C1, D1 and SDL (Figure 1). However, CU AmeriFlux served as an alternate source for GLV4 relative humidity data during years 1998–2000 because of sensor malfunction at the other stations. In both watersheds, observed values of air temperature and wind speed were spatially distributed on the basis of the observed lapse rate each hour, solved as a linear function of elevation [*Molotch et al.*, 2008]. Residuals (i.e., observed minus lapsed values) at each station were spatially distributed using inverse distance-squared weighting. This method was also used to distribute precipitation data across GLV4 because there were multiple observations at different elevations available (unlike for TOK). Relative humidity values were spatially distributed each hour by converting to specific humidity, lapsing to elevation, distributing residuals, and then converting back to relative humidity [*Molotch*, 2009; *Cline et al.*, 1998]. For times when fewer than two stations were operational, average lapse rates for the study period were used. Because the meteorological stations do not cover the entire elevation range of the watersheds, lapse rates were extrapolated over about half of the watersheds (Table 1). New snowfall at each grid cell, used for updating modeled snow albedo, was determined from observed precipitation and a multiplying factor, representing the fraction of precipitation as snow, that ramps linearly from 1 to 0 between an air temperature of -1 and 3°C [*U.S. Army Corps of Engineers*, 1956, plate 3-1]. To evaluate potential errors in the interpolated model forcings, observed values of air temperature, water vapor pressure and wind speed at each station were compared to values obtained via the aforementioned interpolation between the other stations (i.e., "jackknifing") [*Molotch*, 2009].

A2. Shortwave Radiation

[36] Grid cell values (30 m resolution) of downwelling shortwave radiation were estimated by downscaling hourly 0.5° resolution (~44 × 56 km) product from the Geostationary Operational Environmental Satellite (GOES) [*Pinker and Lazlo*, 1992] using TOPORAD v 2.1 [*Dozier and Frew*, 1990; *Dozier*, 1980] and the downscaling procedure of *Molotch* [2009]. TOPORAD was used in order to simulate the effects of terrain aspect, slope, and sky view factors on incident shortwave radiation. The downscaling approach normalizes the radiation grid from TOPORAD so that its spatial mean value equals the value from GOES. We used constant atmospheric input parameters for TOPORAD (see below), and relied on the GOES data to capture the temporal variability in atmospheric conditions. Errors are disclosed with the use of pyranometer measurements. Grid cell albedo values for input to TOPORAD were obtained by area weighting of albedo values for snow-covered and snow-free areas:

$$\alpha = \alpha_{\mathrm{SNOW}}(\mathrm{FSCA}) + \alpha_{\mathrm{ROCK}}(1 - \mathrm{FSCA}), \qquad \text{(A1)}$$

where α is the albedo, α_{ROCK} and α_{SNOW} are the albedos of snow-free and snow-covered areas, respectively, and FSCA is the fractional snow-covered area (described below). The α_{SNOW} was estimated using the Biosphere-Atmosphere Transfer Scheme (BATS), which models snow albedo as a combination of a decay process based on snow age (assumed to represent grain growth and soot) and a recovery process based on new snowfall [*Dickinson et al.*, 1993]. A constant α_{ROCK} value of 0.19 was used in all model simulations on the basis of average reflectance values for granite and granodiorite [*Baldridge et al.*, 2009]. Downwelling shortwave radiation was adjusted for forest cover using the nonlinear transmission function of *Cline and Carroll* [1999] (note that canopy is only present in 5% of western TOK and is not present in GLV4).

[37] The model parameters for the TOPORAD solar radiation model include (clear sky) optical depth (τ), single scattering albedo (ω), scattering asymmetry factor (g), and albedo (described above); the former three parameters were held as constants. Estimates in these 3 parameters for GLV4 were found by fitting the observed transmittance values at station C1 to the analytic solution of the two-stream equations of *Dozier* [1989]. Using the ten best fit days in 1996 and 2002 (20 days total), we obtained τ, ω, and g values of 0.20, 0.53, and 0.37, respectively. When applied to TOK, this procedure produced poor results. Hence, τ, ω, and g were adopted from values for a U.S. Standard atmosphere with rural background aerosol, weighted by the solar radiance in each Landsat band [*Dozier*, 1989]. Model errors in downwelling shortwave radiation were determined using measured values at stations EML and TPL in TOK and stations C1 and SDL in GLV. Shortwave measurements in TOK were made using Eppley PSP pyranometers, and in GLV using Licor pyranometers [*Williams et al.*, 1999].

A3. Longwave Radiation

[38] Grid cell values of longwave radiation were determined using the Stefan-Boltzmann equation. Atmospheric emissivity was derived from observed air temperature,

water vapor pressure, and the "Wachtmann correction" [*Idso*, 1981; *Hodges et al.*, 1983, equation (20)]. In the forested areas of TOK (5%), atmospheric emissivity values were adjusted for the forest canopy [*Cline and Carroll*, 1999]. Upwelling longwave radiation was determined assuming a snow emissivity of 0.98 [*Dozier and Painter*, 2004] and the aforementioned estimates of snow surface temperature. Errors in modeled downwelling longwave radiation were determined using measurements at station SUBNIV in GLV (Kipp & Zonen CG2 pyrgeometer), and stations EML and TPL in TOK (Eppley PIR pyrgeometers).

A4. Turbulent Fluxes

[39] Sensible and latent heat fluxes were computed using a formulation employing bulk transfer coefficients of *Jordan* [1991], with a bulk Richardson number from equation (A18) of *Liston et al.* [1999]. Stability corrections were applied during both unstable and stable turbulent conditions. The reference heights for wind, air temperature and relative humidity were constant values of 5.7, 5.4, and 5.4 m, respectively, for TOK and 7.0, 1.8, and 1.8 m, respectively, for GLV4 (values differ between watersheds because they were instrumented as a part of different projects). A snow surface roughness length of 0.0005 m was used for both watersheds [*Morris*, 1989]. The net turbulent flux is defined as the sum of the sensible and latent heat fluxes; similarly, net radiative flux is the sum of the net shortwave and net longwave radiation. The convention used for expressing the proportion of net turbulent and net radiative flux to total energy of snowmelt follows that used by *Marks and Dozier* [1992]. The percentage of net radiative (turbulent) flux was found by dividing the absolute value of the net radiative (turbulent) flux by the sum of the absolute values of the net radiative and net turbulent fluxes. Turbulent flux measurements were not available for model validation.

Appendix B: Spatial Distribution of Observed Snow Depth in TOK, 2000–2007

[40] After year 1999, the number of depth measurements during the TOK snow surveys ranged from 11 (in 2000) to 95 (in 2002) and averaged 58 (Table 2). This sampling was deemed inadequate for using the binary regression tree method to spatially distribute measurements. Instead, the following approach was used for years after 1999. The average snow depth grid for years 1996–1999, $\overline{d}_{ij}$, was formed by adding the grids (without FSCA masking) and dividing by the number of years (=4), where indices i and j denote the x and y grid coordinates. We then sampled $\overline{d}_{ij}$ at each measurement location of the post-1999 survey, denoting the resulting samples as $\overline{d}_k$, with k ranging from 1 to the total number of depth measurements. Likewise, we defined d_k to be the snow depth measured at location k of the post-1999 survey. We fit the values of d_k and $\overline{d}_k$ to a straight line to solve for the multiplier, c:

$$d_k = c\,\overline{d}_k \tag{B1}$$

The value of c is the average ratio of snow depth at a specific location to the snow depth at that same location on the multiyear grid. Finally, we obtained the desired snow depth grid, d_{ij}, from the product $c\,\overline{d}_{ij}$. We compared the errors in the estimate of mean snow depth with and without the use of the snow depth pattern (i.e., equation (B1)) by performing a hundredfold cross-validation study applied to the 1996–1999 data set. For each year of the 1996–1999 period, 100 training sets of 58 observations (i.e., the mean sample number during years after 1999) were randomly selected. Snow depth grids were generated using these training sets and the method above. Estimates of mean snow depth without the use of patterns were obtained by averaging all observations in the training set. The "true" snow depth was taken to be the average of the entire population of measurements for the year. Mean depth errors without patterns were +2 to +6% (too high), whereas estimates with patterns were −2 to +1%. Thus, use of the snow depth pattern removed much of the positive bias from simple averaging of depth measurements.

[41] **Acknowledgments.** Technical support was provided by the following individuals: S. Burns, N. Caine, T. Erickson, M. Colee, J. M. Melack, K. Musselman, T. H. Painter, and K. Skeen. Helpful commentary on the manuscript was provided by D. W. Clow, D. I. Stannard, and 3 anonymous reviewers. Financial support was provided by NSF grants EAR 1032308, 1032295, 0614207, 0724960, 0738780, 0738930, NASA Grant NNX08AH18G, The NASA Postdoctoral Program, The USGS Mendenhall Research Fellowship Program, the Niwot Ridge LTER program, and NSF's Boulder Creek Critical Zone Observatory. Any use of trade, firm, or product names is for descriptive purposes only and does not imply endorsement by the U.S. Government.

References

Anderson, E. A. (1976), A point energy and mass balance model of a snow cover, *NOAA Tech. Rep. NWS 19*, NOAA, Silver Spring, Md.

Anderton, S. P., S. M. White, and B. Alvera (2004), Evaluation of spatial variability in snow water equivalent for a high mountain catchment, *Hydrol. Processes*, *18*, 435–453.

Arnell, N. W. (1999), Climate change and global water resources, *Global Environ. Change*, *9*, S31–S49.

Baldridge, A. M., S. J. Hook, C. I. Grove, and G. Rivera (2009), The ASTER spectral library version 2.0, *Remote Sens. Environ.*, *113*(4), 711–715.

Bales, R. C., N. P. Molotch, T. H. Painter, M. D. Dettinger, R. Rice, and J. Dozier (2006), Mountain hydrology of the western United States, *Water Resour. Res.*, *42*, W08432, doi:10.1029/2005WR004387.

Barnett, T. P., J. C. Adam, and D. P. Lettenmaier (2005), Potential impacts of a warming climate on water availability in snow-dominated regions, *Nature*, *438*, 303–309.

Brooks, P. D., and M. W. Williams (1999), Snowpack controls on nitrogen cycling and export in seasonally snow-covered catchments, *Hydrol. Processes*, *13*, 2177–2190.

Brubaker, K., A. Rango, and W. Kustas (1996), Incorporating radiation inputs into the snowmelt runoff model, *Hydrol. Processes*, *10*, 1329–1343.

Bunting, L., P. R. Leavitt, R. P. Weidman, and R. D. Vinebrooke (2010), Regulation of the nitrogen biogeochemistry of mountain lakes by subsidies of terrestrial dissolved organic matter and the implications for climate studies, *Limnol. Oceanogr.*, *55*(1), 333–345.

Cayan, D. R. (1996), Interannual climate variability and snowpack in the western United States, *J. Clim.*, *9*, 928–948.

Cayan, D. R., S. A. Kammerdiener, M. D. Dettinger, J. M. Caprio, and D. H. Peterson (2001), Changes in the onset of spring in the western United States, *Bull. Am. Meteorol. Soc.*, *82*(3), 399–415.

Cline, D. (1995), Snow surface energy exchanges and snowmelt at a continental alpine site, in *Biogeochemistry of Seasonally Snow-Covered Catchments, IAHS Publ., 228*, edited by K. A. Tonnessen, M. W. Williams, and M. Tranter, 157–166, Int. Assoc. of Hydrol. Sci., Wallingford, UK.

Cline, D. W., and T. R. Carroll (1999), Inference of snow cover beneath obscuring clouds using optical remote sensing and a distributed snow energy and mass balance model, *J. Geophys. Res.*, *104*(D16), 19,631–19,644.

Cline, D. W., R. C. Bales, and J. Dozier (1998), Estimating the spatial distribution of snow in mountain basins using remote sensing and energy balance modeling, *Water Resour. Res.*, *34*(5), 1275–1285.

Clow, D. W. (2010), Changes in the timing of snowmelt and streamflow in Colorado: A response to recent warming, *J. Clim.*, *23*(9), 2293–2306.

Dickinson, R. E., A. Henderson-Sellers, and P. J. Kennedy (1993), Biosphere-Atmosphere Transfer Scheme (BATS) Version 1e as coupled to the NCAR Community Climate Model, in *NCAR Tech. Note NCAR/TN-387+STR*, 72 pp., Natl. Cent. for Atmos. Res., Boulder, Colo.

Dozier, J. (1980), A clear-sky spectral solar radiation model for snow-covered mountainous terrain, *Water Resour. Res.*, *16*(4), 709–718.

Dozier, J. (1989), Spectral signature of alpine snow cover from the Landsat Thematic Mapper, *Remote Sens. Environ.*, *28*, 9–22.

Dozier, J., and J. Frew (1990), Rapid calculation of terrain parameters for radiation modeling from digital elevation data, *IEEE Trans. Geosci. Remote Sens.*, *28*(5), 963–969.

Dozier, J., and T. H. Painter (2004), Multispectral and hyperspectral remote sensing of alpine snow properties, *Annu. Rev. Earth Planet. Sci.*, *32*, 465–494.

Elder, K., J. Dozier, and J. Michaelsen (1991), Snow accumulation and distribution in an alpine watershed, *Water Resour. Res.*, *27*(7), 1541–1552.

Elder, K., J. Michaelsen, and J. Dozier (1995), Small basin modeling of snow water equivalence using binary regression tree methods, in *Biogeochemistry of Seasonally Snow-Covered Catchments, IAHS Publ., 228*, edited by K. A. Tonnessen, M. W. Williams, and M. Tranter, 129–139, Int. Assoc. of Hydrol. Sci., Wallingford, UK.

Erickson, T. A., M. W. Williams, and A. Winstral (2005), Persistence of topographic controls on the spatial distribution of snow in rugged mountain terrain, Colorado, United States, *Water Resour. Res.*, *41*, W04014, doi:10.1029/2003WR002973.

Gleick, P. H. (1987), Regional hydrologic consequences of increases in atmospheric CO_2 and other trace gases, *Clim. Change*, *10*(2), 137–160.

Hodges, D. B., G. J. Higgins, P. F. Hilton, R. E. Hood, R. Shapiro, C. N. Touart, and R. F. Wachtmann (1983), Final tactical decision aid (FTDA) for infrared (8–12 micron) systems—Technical background, *Rep. AFGL-TR-83-0022*, Air Force Geophys. Lab., Hanscom AFB, Mass.

Huth, A. K., A. Leydecker, J. O. Sickman, and R. C. Bales (2004), A two-component hydrograph separation for three high-elevation catchments in the Sierra Nevada, California, *Hydrol. Processes*, *18*(9), 1721–1733.

Idso, S. B. (1981), A set of equations for full spectrum and 8- to 14-micron and 10.5- to 12.5-micron thermal radiation from cloudless skies, *Water Resour. Res.*, *17*(2), 295–304.

Jefferson, A., A. Nolin, S. Lewis, and C. Tague (2008), Hydrogeologic controls on streamflow sensitivity to climate variation, *Hydrol. Processes*, *22*, 4371–4385.

Jordan, R. (1991), A one-dimensional temperature model for a snow cover, *Spec. Rep. 91-16*, U.S. Army Cold Reg. Res. and Eng. Lab., Hanover, N. H.

Judson, A., and N. Doesken (2000), Density of freshly fallen snow in the central Rocky Mountains, *Bull. Am. Meteorol. Soc.*, *81*(7), 1577–1587.

Kattelmann, R., and K. Elder (1991), Hydrologic characteristics and water balance of an alpine basin in the Sierra Nevada, *Water Resour. Res.*, *27*(7), 1553–1562.

Knowles, N., and D. R. Cayan (2004), Elevational dependence of projected hydrologic changes in the San Francisco Estuary and watershed, *Clim. Change*, *62*, 319–336.

Lehning, M., I. Völksch, D. Gustafsson, T. A. Nguyen, M. Stähli, and M. Zappa (2006), ALPINE3D: A detailed model of mountain surface processes and its application to snow hydrology, *Hydrol. Processes*, *20*, 2111–2128.

Leydecker, A., J. O. Sickman, and J. M. Melack (2001), Spatial scaling of hydrological and biogeochemical aspects of high-elevation catchments in the Sierra Nevada, California, U.S.A., *Arct. Antarct. Alp. Res.*, *33*, 391–396.

Liston, G. E., J.-G. Winther, O. Bruland, H. Elvehøy, and K. Sand (1999), Below-surface ice melt on the coastal Antarctic ice sheet, *J. Glaciol.*, *45*(150), 273–285.

Liu, F., M. W. Williams, and N. Caine (2004), Source waters and flow paths in an alpine catchment, Colorado Front Range, United States, *Water Resour. Res.*, *40*, W09401, doi:10.1029/2004WR003076.

Luce, C. H., D. G. Tarboton, and K. R. Cooley (1998), The influence of the spatial distribution of snow on basin-averaged snowmelt, *Hydrol. Processes*, *12*, 1671–1683.

Male, D. H., and R. J. Granger (1981), Snow surface energy exchange, *Water Resour. Res.*, *17*(3), 609–627.

Marks, D., and J. Dozier (1992), Climate and energy exchange at the snow surface in the alpine region of the Sierra Nevada: 2. Snow cover energy balance, *Water Resour. Res.*, *28*(11), 3043–3054.

Marks, D., J. Dozier, and R. E. Davis (1992), Climate and energy exchange at the snow surface in the alpine region of the Sierra Nevada: 1. Meteorological measurements and monitoring, *Water Resour. Res.*, *28*(11), 3029–3042.

Martinec, J., and A. Rango (1981), Areal distribution of snow water-equivalent evaluated by snow cover monitoring, *Water Resour. Res.*, *17*(5), 1480–1488.

Meixner, T., R. C. Bales, M. W. Williams, D. H. Campbell, and J. S. Baron (2000), Stream chemistry modeling of two watersheds in the Front Range, Colorado, *Water Resour. Res.*, *36*(1), 77–87.

Melack, J. M., and J. O. Sickman (1995), Snowmelt induced chemical changes in seven streams in the Sierra Nevada, California, in *Biogeochemistry of Seasonally Snow-Covered Catchments, IAHS Publ., 228*, edited by K. A. Tonnessen, M. W. Williams, and M. Tranter, 221–234, Int. Assoc. of Hydrol. Sci., Wallingford, UK.

Molotch, N. P. (2009), Reconstructing snow water equivalent in the Rio Grande headwaters using remotely sensed snow cover data and a spatially distributed snowmelt model, *Hydrol. Processes*, *23*(7), 1076–1089.

Molotch, N. P., and R. C. Bales (2006), Comparison of ground-based and airborne snow surface albedo parameterizations in an alpine watershed: Impact on snowpack mass balance, *Water Resour. Res.*, *42*, W05410, doi:10.1029/2005WR004522.

Molotch, N. P., and S. A. Margulis (2008), Estimating the distribution of snow water equivalent using remotely sensed snow cover data and a spatially distributed snowmelt model: A multi-resolution, multi-sensor comparison, *Adv. Water Resour.*, *31*, 1503–1514.

Molotch, N. P., S. R. Fassnacht, R. C. Bales, and S. R. Helfrich (2004), Estimating the distribution of snow water equivalent and snow extent beneath cloud cover in the Salt-Verde River basin, Arizona, *Hydrol. Processes*, *18*, 1595–1611.

Molotch, N. P., M. T. Colee, R. C. Bales, and J. Dozier (2005), Estimating the spatial distribution of snow water equivalent in an alpine basin using binary regression tree models: The impact of digital elevation data and independent variable selection, *Hydrol. Processes*, *19*, 1459–1479.

Molotch, N. P., T. Meixner, and M. W. Williams (2008), Estimating stream chemistry during the snowmelt pulse using a spatially distributed, coupled snowmelt and hydrochemical modeling approach, *Water Resour. Res.*, *44*, W11429, doi:10.1029/2007WR006587.

Molotch, N. P., S. A. Margulis, and S. M. Jepsen (2010), Response to comment by A. G. Slater, M. P. Clark, and A. P. Barrett on "Estimating the distribution of snow water equivalent using remotely sensed snow cover data and a spatially distributed snowmelt model: A multi-resolution, multi-sensor comparison," *Adv. Water Resour.*, *33*(2), 231–239.

Morris, E. M. (1989), Turbulent transfer over snow and ice, *J. Hydrol.*, *105*, 205–223.

Nash, J. E., and J. V. Sutcliffe (1970), River flow forecasting through conceptual models, part 1—A discussion of principles, *J. Hydrol.*, *10*(3), 282–290.

Painter, T. H., K. Rittger, C. McKenzie, P. Slaughter, R. E. Davis, and J. Dozier (2009), Retrieval of subpixel snow covered area, grain size, and albedo from MODIS, *Remote Sens. Environ.*, *113*, 868–879.

Pinker, R. T., and I. Laszlo (1992), Modeling surface solar irradiance for satellite applications on a global scale, *J. Appl. Meteorol.*, *31*, 194–211.

Pohl, S., P. Marsh, and G. E. Liston (2006), Spatial-temporal variability in turbulent fluxes during spring snowmelt, *Arct. Antarct. Alp. Res.*, *38*(1), 136–146.

Pomeroy, J. W., D. M. Gray, K. R. Shook, B. Toth, R. L. H. Essery, A. Pietroniro, and N. Hedstrom (1998), An evaluation of snow accumulation and ablation processes for land surface modeling, *Hydrol. Processes*, *12*, 2339–2367.

Rosenthal, W., and J. Dozier (1996), Automated mapping of montane snow cover at subpixel resolution from the Landsat Thematic Mapper, *Water Resour. Res.*, *32*(1), 115–130.

Serreze, M. C., M. P. Clark, R. L. Armstrong, D. A. McGinnis, and R. S. Pulwarty (1999), Characteristics of the western United States snowpack from snowpack telemetry (SNOTEL) data, *Water Resour. Res.*, *35*(7), 2145–2160.

Sickman, J. O., A. Leydecker, and J. M. Melack (2001), Nitrogen mass balance and abiotic controls on N retention and yield in high-elevation catchments of the Sierra Nevada, California, United States, *Water Resour. Res.*, *37*(5), 1445–1461.

Stephenson, N. (1988), Climatic record of vegetation distribution: The role of the water balance with examples from North America and Sequoia National Park, California, PhD dissertation, Cornell Univ., Ithaca, N. Y.

Stewart, I. T., D. R. Cayan, and M. D. Dettinger (2005), Changes toward earlier streamflow timing across western North America, *J. Clim.*, *18*(8), 1136–1155.

Tague, C., and G. E. Grant (2009), Groundwater dynamics mediate low-flow response to global warming in snow-dominated alpine regions, *Water Resour. Res.*, *45*, W07421, doi:10.1029/2008WR007179.

Tonnessen, K. A. (1991), The Emerald Lake watershed study: Introduction and site description, *Water Resour. Res.*, *27*(7), 1537–1539.

U.S. Army Corps of Engineers (1956), *Snow Hydrology: Summary Report of the Snow Investigations*, North Pac. Div., Portland, Oreg.

Williams, M. W., and J. M. Melack (1991a), Solute chemistry of snowmelt and runoff in an alpine basin, Sierra Nevada, *Water Resour. Res.*, *27*(7), 1575–1588.

Williams, M. W., and J. M. Melack (1991b), Precipitation chemistry in and ionic loading to an alpine basin, Sierra Nevada, *Water Resour. Res.*, *27*(7), 1563–1574.

Williams, M. W., M. Losleben, N. Caine, and D. Greenland (1996), Changes in climate and hydrochemical responses in a high-elevation catchment in the Rocky Mountains, USA, *Limnol. Oceanogr.*, *41*(5), 939–946.

Williams, M. W., D. Cline, M. Hartmann, and T. Bardsley (1999), Data for snowmelt model development, calibration, and verification at an alpine site, Colorado Front Range, *Water Resour. Res.*, *35*(10), 3205–3209.

Williams, M. W., D. Helmig, and P. Blanken (2009), White on green: Under-snow microbial processes and trace gas fluxes through snow, Niwot Ridge, Colorado Front Range, *Biogeochemistry*, *95*(1), 1–12.

Williams, M. W., R. T. Barnes, J. N. Parman, M. Freppaz, and E. Hood (2011), Stream water chemistry along an elevational gradient from the Continental Divide to the foothills of the Rocky Mountains, *Vadose Zone J.*, *10*, 900–914.

Winstral, A., K. Elder, and R. E. Davis (2002), Spatial snow modeling of wind-redistributed snow using terrain-based parameters, *J. Hydrometeorol.*, *3*(5), 524–538.

S. M. Jepsen, U.S. Geological Survey, Box 25046, Denver Federal Center, Denver, CO 80225, USA.

N. P. Molotch and M. W. Williams, Institute of Arctic and Alpine Research, University of Colorado at Boulder, 1560 30th St., Boulder, CO 80303, USA. (noah.molotch@colorado.edu)

K. E. Rittger, Donald Bren School of Environmental Science and Management, University of California, Santa Barbara, CA 93106-5131, USA.

J. O. Sickman, Department of Environmental Sciences, University of California, Riverside, CA 92521, USA.